

K_1/K^* enhancement as a signature of chiral symmetry restoration in heavy ion collisions

Hae-Som Sung,^{1,*} Sungtae Cho,^{2,†} Juhee Hong,^{1,‡} Su Houng Lee,^{1,§} Sanghoon Lim,^{3,¶} and Taesoo Song^{4,**}

¹*Department of Physics and Institute of Physics and Applied Physics, Yonsei University, Seoul 03722, Korea*

²*Division of Science Education, Kangwon National University, Chuncheon 24341, Korea*

³*Department of Physics, Pusan National University, Pusan, Korea*

⁴*GSI Helmholtzzentrum für Schwerionenforschung GmbH, Planckstrasse 1, 64291 Darmstadt, Germany*

Based on the fact that the mass difference between the chiral partners is an order parameter of chiral phase transition and that the chiral order parameter reduces substantially at the chemical freeze-out point in ultra-relativistic heavy ion collisions, we argue that the production ratio of K_1 over K^* in such collisions should be substantially larger than that predicted in the statistical hadronization model. We further show that while the enhancement effect might be contaminated by the relatively larger decrease of K_1 meson than K^* meson during the hadronic phase, the signal will be visible through a systematic study on centrality as the kinetic freeze-out temperature is higher and the hadronic life time shorter in peripheral collisions than in central collisions.

I. INTRODUCTION

A recent lattice calculation finds the pseudo-critical temperature for QCD chiral crossovers at zero baryon chemical potential to be around 156.5 ± 1.5 MeV [1], a value that is consistent with previous results [2]. This temperature is close to the chemical freeze-out temperature obtained from the statistical hadronization model analysis based on the yields of hadrons produced in heavy ion collisions at both Relativistic Heavy Ion Collider (RHIC) and Large Hadron Collider (LHC) [3, 4]. Near this temperature, the chiral order parameter associated with the transition is substantially reduced from its vacuum value [5]. While the quark condensate is the standard chiral order parameter, so is the difference between the vector and axial vector correlation function. That is to say, the mass difference between the ρ and a_1 is due to the chiral symmetry breaking as is well represented in the Weinberg relation [6]. Hence, when hadrons are produced at the chemical freeze-out point in heavy ion collisions, the chiral partners will have masses much closer to each other than their vacuum values. This does not mean that the masses should vanish at the chemical freeze-out point. In fact, a recent study shows that while chiral symmetry breaking is responsible for the mass difference between the ρ and a_1 meson, it only accounts for a small fraction of the common mass [7].

Statistical hadronization model analysis indicates that the abundances of hadrons are determined at the chemical freeze-out point [8]. This suggests that the production of chiral partners at the chemical freeze-out point will be similar. Unfortunately, a_1 has a large vacuum decay width and a large dissociation cross section so that

many of the a_1 produced at the chemical freeze-out will not survive during the hadronic phase. Indeed, the measured yields of resonances with large decay widths tend to be smaller than the statistical hadronization model predictions.

On the other hand, recently it has been emphasized by one of us that the K_1 and K^* are also chiral partners and that both have vacuum widths that are smaller than 100 MeV, making them ideal objects to study the effects of partial chiral symmetry restoration in a nuclear target experiment [9]. In this work, we will show that the enhancement of the ratio K^1/K^* in heavy ion collisions can be used as a signature of chiral symmetry restoration in the early stages of heavy ion collisions. Effects of chiral symmetry restoration in heavy ion collisions were studied in K^+/π^+ , $(\Lambda + \Sigma^0)/\pi^-$ ratios [10]. Here, we will study the K^1/K^* ratio as their properties are direct order parameters of spontaneous chiral symmetry breaking.

II. K_1, K^* COUPLINGS IN AN EFFECTIVE LAGRANGIAN

From a symmetry argument alone, one expects K_1 to be the chiral partner of K^* . In fact, arguments based solely on chiral symmetry predict that when chiral symmetry is restored, the vector and axial particles become degenerate [11]. For these effects to be observable in heavy ion collisions, the vacuum widths as well as the hadronic dissociation of both vector and axial particles should be small so that the signal will not be smeared out during the hadronic phase. Since the vacuum widths of both the K_1 and K^* meson are already smaller than 100 MeV, we focus here on their hadronic absorptions during the hadronic phase as well as on the centrality dependence of these effects in a heavy ion collision. Still, in order to work out the suppression of the initially produced K_1 mesons during the hadronic phase of heavy ion collisions, we need to estimate the hadronic cross sections with other hadrons.

* ioussom@yonsei.ac.kr

† sungtae.cho@kangwon.ac.kr

‡ juhehong@yonsei.ac.kr

§ suhoung@yonsei.ac.kr

¶ shlim@pusan.ac.kr

** t.song@gsi.de

For that purpose, we use the Lagrangian involving spin-1 and spin-0 mesons following the massive Yang-Mills approach [12]:

$$\begin{aligned} \mathcal{L}_V = & \frac{1}{8} F_\pi^2 \text{Tr} (D_\mu U D^\mu U^\dagger) + \frac{1}{8} F_\pi^2 \text{Tr} [M (U + U^\dagger - 2)] \\ & - \frac{1}{2} \text{Tr} (F_{\mu\nu L} F_L^{\mu\nu} + F_{\mu\nu R} F_R^{\mu\nu}) \\ & + m_0^2 \text{Tr} (A_{\mu L} A_L^\mu + A_{\mu R} A_R^\mu), \end{aligned} \quad (1)$$

where $U = \exp(2iP/\sqrt{2}f_\pi)$ with the octet of pseudoscalar mesons $P = P^a \lambda^a / \sqrt{2}$ and $F_\pi = \sqrt{2}f_\pi = 132$ MeV. The covariant derivative and the field strength tensor are given by

$$\begin{aligned} D_\mu U &= \partial_\mu U - ig A_{\mu L} U + ig U A_{\mu R}, \\ F_{\mu\nu}^{L,R} &= \partial_\mu A_\nu^{L,R} - \partial_\nu A_\mu^{L,R} - ig [A_\mu^{L,R}, A_\nu^{L,R}], \end{aligned} \quad (2)$$

where $V_\mu = A_\mu^L + A_\mu^R$ and $A_\mu = A_\mu^L - A_\mu^R$ with the vector and axial-vector mesons $V_\mu = V_\mu^a \lambda^a / \sqrt{2}$ and $A_\mu = A_\mu^a \lambda^a / \sqrt{2}$.

From the first term of Eq. (1), we can read off the $K^* K \pi$ and the $K_1 K \rho$ interaction terms.

$$\begin{aligned} \mathcal{L}^{(3)} = & \frac{ig}{2} \text{Tr} (V_\mu P \overleftrightarrow{\partial}^\mu P) \\ & + \frac{ig^2 F_\pi}{4} \text{Tr} (V_\mu P A^\mu - V_\mu A^\mu P) \\ & + \frac{ig}{2} \text{Tr} [(\partial_\mu V_\nu - \partial_\nu V_\mu) V^\mu V^\nu] \\ & + ig \text{Tr} [(\partial_\mu V_\nu - \partial_\nu V_\mu) A^\mu A^\nu - \partial_\nu A_\mu A^\mu V^\nu]. \end{aligned} \quad (3)$$

Specifically,

$$\begin{aligned} \mathcal{L}_{VPP} = & \frac{ig}{2} \bar{K}^{*\mu} [(\vec{\tau} \cdot \partial_\mu \vec{\pi}) K - (\vec{\tau} \cdot \vec{\pi}) \partial_\mu K] \\ & + \frac{ig}{2} \bar{K} [(\vec{\tau} \cdot \vec{\rho}^\mu)] \partial_\mu K + H.C., \\ \mathcal{L}_{AVP} = & i \frac{g^2 F_\pi}{4} \bar{K}_1^\mu [(\vec{\tau} \cdot \vec{\rho}_\mu) K - (\vec{\tau} \cdot \vec{\pi}) K_\mu^*] + H.C., \end{aligned} \quad (4)$$

with $K \equiv (K^+, K^0)^T$, $K^* \equiv (K^+, K^{*0})^T$ and $K_1 \equiv (K_1^+, K_1^0)^T$ being the strange pseudoscalar, vector and axial-vector meson isospin doublets, respectively. $\vec{\pi}$ and $\vec{\rho}$, with Pauli matrices $\vec{\tau}$, are the pion and ρ meson isospin triplets.

As it stands, the interaction terms for $K_1 K^* \pi$ and $K_1 K \rho$ have a common coupling as given from Eq. (3). This leads to a larger calculated decay width of $K_1 K^* \pi$ compared with that of $K_1 K \rho$, because the phase space for the former two-body decay is larger than that for the latter. On the other hand, experimentally one finds $\Gamma_{K_1 \rightarrow K^* \pi} = 25$ MeV and $\Gamma_{K_1 \rightarrow K \rho} = 38$ MeV. The resolution of this puzzles comes from mixing effects. In the vacuum, the low-lying modes that couple to the vector current are $K^*(892)$ and $K^*(1410)$ while those for the axial vector current are $K_1(1270)$ and $K_1(1400)$. There is a subtlety in the nature of the two K_1 states: they

are assumed to be a mixture of the 3P_1 and 1P_1 quark-antiquark pair in the quark model [13]. We therefore introduce two mixing angles θ_A and θ_V so that the chiral Lagrangian in Eq. (4) and (5) are constructed for both (K_A^*, K_{1A}) and (K_B^*, K_{1B}) that are related to the physical mesons as follows:

$$\begin{aligned} K_{1A} &= \cos \theta_A K_1(1270) + \sin \theta_A K_1(1400), \\ K_{1B} &= -\sin \theta_A K_1(1270) + \cos \theta_A K_1(1400), \\ K_A^* &= \cos \theta_V K^*(892) + \sin \theta_V K^*(1410), \\ K_B^* &= -\sin \theta_V K^*(892) + \cos \theta_V K^*(1410). \end{aligned} \quad (6)$$

Now, we re-express the sum of the two chiral Lagrangians in terms of K_1 and K^* mesons and the two independent couplings g_A, g_B so that the SU(2) chiral symmetry is still preserved.

$$\begin{aligned} \mathcal{L}'_{VPP} = & ig_{K^* K \pi} \bar{K}^{*\mu} \left[(\sqrt{2} \vec{\tau} \cdot \partial_\mu \vec{\pi}) K - (\sqrt{2} \vec{\tau} \cdot \vec{\pi}) \partial_\mu K \right] \\ & + H.C., \end{aligned} \quad (7)$$

$$\begin{aligned} \mathcal{L}'_{AVP} = & ig_{K_1 K \rho} \bar{K}_1^\mu \left(\sqrt{2} \vec{\tau} \cdot \vec{\rho}_\mu \right) K \\ & - ig_{K_1 K^* \pi} \bar{K}_1^\mu \left(\sqrt{2} \vec{\tau} \cdot \vec{\pi} \right) K_\mu^* + H.C., \end{aligned} \quad (8)$$

where

$$\begin{aligned} g_{K^* K \pi} &= \frac{1}{4\sqrt{2}} (g_A \cos \theta_V - g_B \sin \theta_V), \\ g_{K^*(1410) K \pi} &= \frac{1}{4\sqrt{2}} (g_A \sin \theta_V + g_B \cos \theta_V), \\ g_{K_1 K \rho} &= \frac{F_\pi}{8\sqrt{2}} (g_A^2 \cos \theta_A - g_B^2 \sin \theta_A), \\ g_{K_1(1400) K \rho} &= \frac{F_\pi}{8\sqrt{2}} (g_A^2 \sin \theta_A + g_B^2 \cos \theta_A), \\ g_{K_1 K^* \pi} &= \frac{F_\pi}{8\sqrt{2}} (g_A^2 \cos \theta_A \cos \theta_V + g_B^2 \sin \theta_A \sin \theta_V), \\ g_{K_1(1400) K^* \pi} &= \frac{F_\pi}{8\sqrt{2}} (g_A^2 \sin \theta_A \cos \theta_V - g_B^2 \cos \theta_A \sin \theta_V). \end{aligned} \quad (9)$$

Using the above interaction Lagrangians, we determine the mixing angle $\theta_A(\theta_B)$ and coupling constant $g_A(g_B)$ to best fit the experimental data for the six decay processes given in Table I. The table also summarizes the best fit couplings and the experimental data as well as the calculated decay widths of the six processes.

III. THE CROSS SECTION OF THE K_1 MESON

We assume that K_1 mesons are in thermal equilibrium when they are produced at the chemical freeze-out. Then K_1 mesons interact with other particles until the kinetic

ABC	$K^*(892)K\pi$	$K^*(1410)K\pi$	$K_1(1270)K\rho$	$K_1(1400)K\rho$	$K_1(1270)K^*(892)\pi$	$K_1(1400)K^*(892)\pi$
g_{ABC}	3.17	0.9	2.9 (GeV)	-1.02 (GeV)	0.649 (GeV)	-1.95 (GeV)
$\Gamma_{A \rightarrow BC}(\text{experiment})$	50.0 (MeV)	15.6 (MeV)	37.8 (MeV)	5.2 (MeV)	14.4 (MeV)	163 (MeV)
$\Gamma_{A \rightarrow BC}(\text{calculated})$	48.4 (MeV)	14.8 (MeV)	39.7 (MeV)	14.7 (MeV)	9.42 (MeV)	98.6 (MeV)

TABLE I. The coupling constants are calculated with $g_A=15.5$, $g_B=-10.4$, $\cos\theta_V=0.6469$, $\sin\theta_V=0.7626$, $\cos\theta_A=0.724$ and $\sin\theta_A=-0.6898$. With these parameters we also find four point couplings $g_{K_1(1270)K\pi\pi}=7.67(\text{GeV}^{-1})$ and $g_{K_1(1400)K\pi\pi}=-34.5(\text{GeV}^{-1})$.

freeze-out point. We consider the hadronic effect on the K_1 meson due to interactions with light mesons such as pions and rho mesons; $K_1+\pi \rightarrow K+\pi$, $K_1+\pi \rightarrow K^*+\rho$, $K_1+\rho \rightarrow K^*+\pi$, and $K_1+\rho \rightarrow K+\rho$. In addition to the interaction terms given in Eq. (7) and (8), the Lagrangian describing the interaction between the K_1 meson and pions and rho mesons is given as follows:

$$\begin{aligned}
\mathcal{L}'_{APPP} &= 2g_{K_1K\pi\pi}\bar{K}_1^\mu \left[(\vec{\tau} \cdot \partial_\mu \vec{\pi}) (\vec{\tau} \cdot \vec{\pi}) K + (\vec{\tau} \cdot \vec{\pi})^2 \partial_\mu K \right], \\
\mathcal{L}'_{VPP} &= ig_{\rho\pi\pi} [\rho^{0\mu} (\partial_\mu \pi^+ \pi^- - \pi^+ \partial_\mu \pi^-) \\
&\quad + \rho^{+\mu} (\partial_\mu \pi^- \pi^0 - \pi^- \partial_\mu \pi^0) \\
&\quad + \rho^{-\mu} (\partial_\mu \pi^0 \pi^+ - \pi^0 \partial_\mu \pi^+)] + H.C. \\
&\quad + ig_{KK\rho} \left[\bar{K} \left(\sqrt{2} \vec{\tau} \cdot \vec{\rho}^\mu \right) \partial_\mu K - \partial_\mu \bar{K} \left(\sqrt{2} \vec{\tau} \cdot \vec{\rho}^\mu \right) K \right], \\
\mathcal{L}'_{AVP} &= ig_{a_1\rho\pi} \{ \rho^{+\mu} (\pi^- a_{1\mu}^0 - \pi^0 a_{1\mu}^-) \\
&\quad + \rho^{-\mu} (\pi^0 a_{1\mu}^+ - \pi^+ a_{1\mu}^0) + \rho^{0\mu} (\pi^+ a_{1\mu}^- - \pi^- a_{1\mu}^+) \} \\
\mathcal{L}'_{VVV} &= \sqrt{2} ig_{K^*K^*\rho} [\bar{K}^{*\nu} \vec{\tau} K^{*\mu} (\partial_\mu \vec{\rho}_\nu - \partial_\nu \vec{\rho}_\mu) \\
&\quad + (\partial_\mu \bar{K}^{*\nu} - \partial_\nu \bar{K}^{*\mu}) \vec{\tau} \cdot \vec{\rho}^\mu K^{*\nu} \\
&\quad + \bar{K}^{*\mu} \vec{\tau} \cdot \vec{\rho}^\nu (\partial_\mu K_\nu^* - \partial_\nu K_\mu^*)] \\
&\quad + \frac{ig}{2} [(\partial_\mu (\vec{\tau} \cdot \vec{\rho}_\nu) - \partial_\nu (\vec{\tau} \cdot \vec{\rho}_\mu)) (\vec{\tau} \cdot \vec{\rho}^\mu) (\vec{\tau} \cdot \vec{\rho}^\nu)], \\
\mathcal{L}'_{AAV} &= i\sqrt{2} g_{K_1 a_1 K^*} [\partial_\nu \bar{K}_{1\mu} \{ (\vec{a}_{1\nu}^\nu \cdot \vec{\tau}) K^{*\mu} \\
&\quad - (\vec{a}_{1\nu}^\mu \cdot \vec{\tau}) K^{*\nu} \} - \bar{K}_1^\mu \partial_\mu (\vec{a}_{1\nu} \cdot \vec{\tau}) K^{*\nu}] \\
&\quad + i\sqrt{2} g_{K_1 K_1 \rho} [\{ \bar{K}_1^\mu (\vec{\rho}^\nu \cdot \vec{\tau}) - \bar{K}_1^\nu (\vec{\rho}^\mu \cdot \vec{\tau}) \} \partial_\nu K_{1\mu} \\
&\quad - ig \partial_\mu \bar{K}_1^\nu (\vec{\rho}_\nu \cdot \vec{\tau}) K_{1\mu}^\nu]. \tag{10}
\end{aligned}$$

The coupling constant $g = 8.49$ is determined by fitting the experimental decay width of $\rho \rightarrow \pi\pi$, from which we find $g_{\rho\pi\pi} = g_{\rho\rho\rho} = g/\sqrt{2} = 6.006$ and $g_{KK\rho} = g/2\sqrt{2} = 3.003$. In the strange vector and axial-vector mesons, we apply the mixing angle and coupling constants g_A and g_B , which were determined to give the coupling constants as given in Table I and additionally $g_{K^*K^*\rho} = 0.078$, $g_{K_1K_1\rho} = 1.12$, $g_{K_1 a_1 K^*} = 4.5$ and $g_{a_1\rho\pi} = 3.36$ (GeV).

The amplitude for each scattering of different charge states can be written as two isospin channels because of isospin conservation. For example, the scattering of $\pi K_1 \rightarrow K\pi$ consists of the following charge states :

$K^-\pi^- \rightarrow K_1^-\pi^-$, $K^-\pi^0 \rightarrow K_1^-\pi^0$, $\bar{K}^0\pi^- \rightarrow K_1^-\pi^0$, $K^-\pi^+ \rightarrow K_1^-\pi^+$, and $\bar{K}^0\pi^0 \rightarrow K_1^-\pi^+$. These five processes are described by two independent scattering amplitudes $a_{3/2}$ and $a_{1/2}$ for isospin 3/2 and 1/2 channels, respectively, so that

$$\begin{cases}
\langle K^-\pi^- | S | K_1^-\pi^- \rangle = a_{3/2} \\
\langle K^-\pi^0 | S | K_1^-\pi^0 \rangle = \frac{2}{3}a_{3/2} + \frac{1}{3}a_{1/2} \\
\langle \bar{K}^0\pi^- | S | K_1^-\pi^0 \rangle = -\frac{\sqrt{2}}{3}(a_{3/2} - a_{1/2}) \\
\langle K^-\pi^+ | S | K_1^-\pi^+ \rangle = \frac{1}{3}a_{3/2} + \frac{2}{3}a_{1/2} \\
\langle \bar{K}^0\pi^0 | S | K_1^-\pi^+ \rangle = \frac{\sqrt{2}}{3}(a_{3/2} - a_{1/2})
\end{cases} \quad (11)$$

It should be noted that squaring and adding all five amplitudes, one finds that the sum is proportional to $2a_{3/2}^2 + a_{1/2}^2$ reflecting the degeneracy of the isospin.

Using the interaction terms in the Lagrangian discussed above, we evaluated the amplitudes for all diagrams shown in Fig. 1. These represent the absorption amplitudes of the K_1 meson by π and ρ mesons. First, the amplitudes for K_1 absorption by π mesons are represented by the processes $\pi K_1 \rightarrow \pi K$ and $\pi K_1 \rightarrow \rho K^*$. The amplitude for definite isospin channels of the $\pi(p_1)K_1(p_2) \rightarrow \pi(p_3)K(p_4)$ are given as $a_{1/2} = g_{K_1K\pi\pi}\epsilon_2^\mu (p_1 + 3p_3)_\mu + 3\mathcal{M}_1^s + 2\mathcal{M}_1^t + \mathcal{M}_1^u$ and $a_{3/2} = -2g_{K_1K\pi\pi}\epsilon_2^\mu p_{1\mu} - \mathcal{M}_1^t - 2\mathcal{M}_1^u$ for isospin 1/2 and 3/2, respectively. Here, $\mathcal{M}_1^s = \mathcal{M}_{(1-b)}$, $\mathcal{M}_1^t = \mathcal{M}_{(1-c)}$, and $\mathcal{M}_1^u = \mathcal{M}_{(1-d)}$, where the subscript in the right hand side represents the diagrams in Fig. 1. The matrix elements are given as

$$\begin{aligned}
\mathcal{M}_1^s &= g_{K_1K^*\pi} g_{K^*K\pi} \epsilon_2^\mu (p_3 - p_4)^\nu \\
&\quad \times \frac{-g_{\mu\nu} + (p_1 + p_2)_\mu (p_1 + p_2)_\nu / s}{s - m_{K^*}^2}, \\
\mathcal{M}_1^t &= g_{\rho\pi\pi} g_{K_1K\rho} \epsilon_2^\mu \frac{-(p_1 + p_3)_\mu}{t - m_\rho^2}, \\
\mathcal{M}_1^u &= g_{K_1K^*\pi} g_{K^*K\pi} \epsilon_2^\mu (p_1 + p_4)^\nu \\
&\quad \times \frac{-g_{\mu\nu} + (p_1 - p_4)_\mu (p_1 - p_4)_\nu / u}{u - m_{K^*}^2}. \tag{12}
\end{aligned}$$

The two independent amplitudes for the $\pi(p_1)K_1(p_2) \rightarrow \rho(p_3)K^*(p_4)$ are respectively given as $a_{1/2} = 3\mathcal{M}_2^s + 2\mathcal{M}_2^t +$

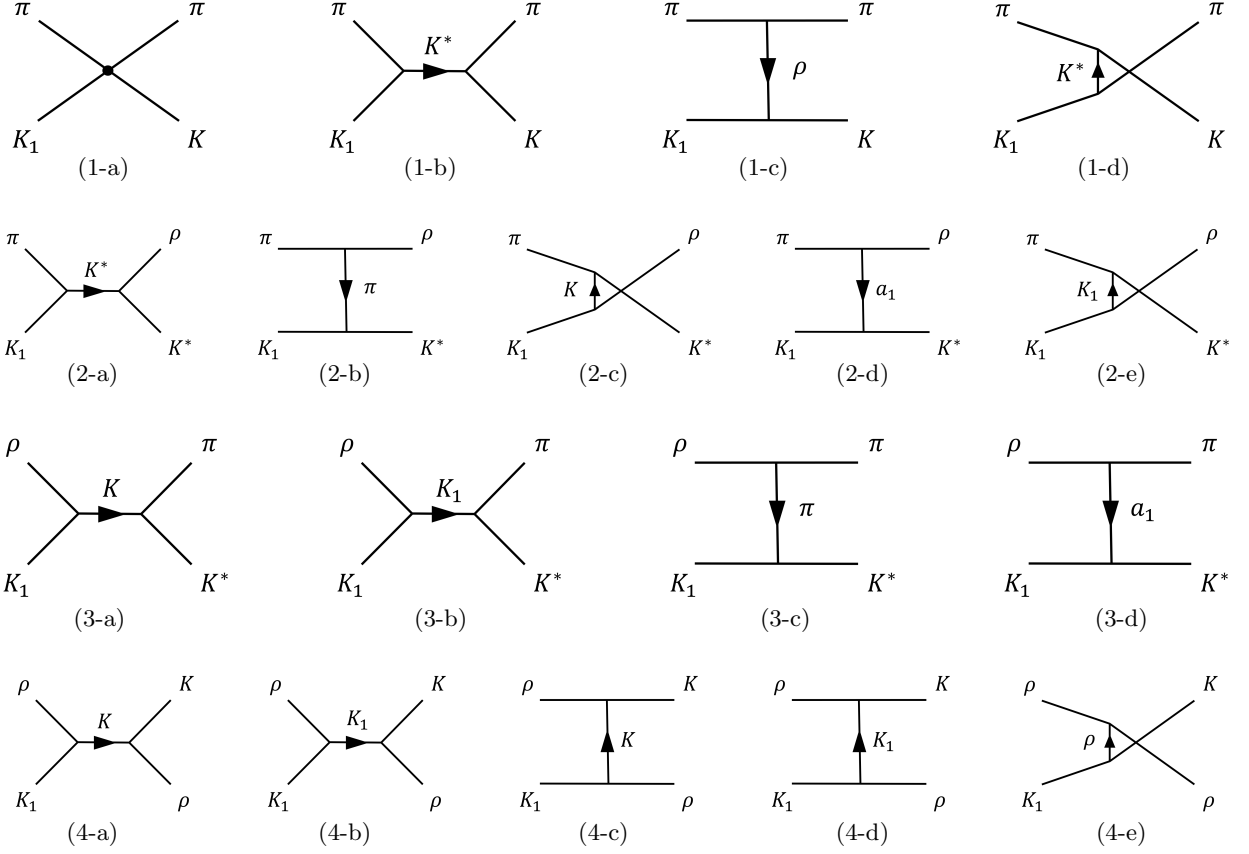


FIG. 1. Feynman diagrams for the K_1 meson absorption by π , ρ mesons. (1) $K_1\pi \rightarrow K\pi$, (2) $K_1\pi \rightarrow K^*\rho$, (3) $K_1\rho \rightarrow K^*\pi$ and (4) $K_1\rho \rightarrow K\rho$.

\mathcal{M}_2^u and $a_{3/2} = -\mathcal{M}_2^t - 2\mathcal{M}_2^u$. Here, $\mathcal{M}_2^t = \mathcal{M}_{(2-b)} + \mathcal{M}_{(2-d)}$ and $\mathcal{M}_2^u = \mathcal{M}_{(2-c)} + \mathcal{M}_{(2-e)}$, with

$$\begin{aligned}
\mathcal{M}_2^s &= g_{K_1 K^* \pi} g_{K^* K^* \rho} \epsilon_2 \alpha^* \epsilon_3^* \epsilon_4^{\delta} \frac{-g^{\alpha\beta} + (p_1 + p_2)^\alpha (p_1 + p_2)^\beta / s}{s - m_{K^*}^2} [g_{\gamma\beta} (2p_3 + p_4)_\delta - g_{\delta\beta} (p_3 + 2p_4)_\gamma - g_{\gamma\delta} (p_3 - p_4)_\beta], \\
\mathcal{M}_2^t &= g_{K_1 K^* \pi} g_{\rho \pi \pi} \epsilon_2^\mu \epsilon_4^* \epsilon_3^* \epsilon_4^{\delta} \frac{1}{t - m_\pi^2} (2p_1 - p_3)_\gamma \\
&\quad + g_{a_1 \rho \pi} g_{K_1 a_1 K^*} \epsilon_2^\mu \epsilon_3^* \epsilon_4^{\delta} \frac{-g^{\alpha\beta} + (p_1 - p_3)^\alpha (p_1 - p_3)^\beta / t}{t - m_{a_1}^2} [g_{\mu\beta} p_{2\delta} - g_{\mu\delta} p_{2\beta} + g_{\beta\delta} (p_1 - p_3)_\mu], \\
\mathcal{M}_2^u &= g_{K_1 K \rho} g_{K^* K \pi} \epsilon_2^\mu \epsilon_3^* \epsilon_4^{\delta} \frac{1}{u - m_\pi^2} (2p_1 - p_4)_\delta \\
&\quad + g_{K_1 K^* \pi} g_{K_1 K_1 \rho} \epsilon_2^\mu \epsilon_3^* \epsilon_4^{\delta} \frac{-g^{\alpha\beta} + (p_1 - p_4)^\alpha (p_1 - p_4)^\beta / u}{u - m_{K_1}^2} [g_{\mu\beta} (p_1 - p_4)_\gamma + g_{\mu\gamma} p_{2\beta} - g_{\gamma\beta} (p_1 - p_4)_\mu].
\end{aligned} \tag{13}$$

Second, the amplitudes for absorption by ρ mesons are $\rho K_1 \rightarrow \pi K^*$ and $\rho K_1 \rightarrow K\rho$. The isospin channels of $\rho(p_1)K_1(p_2) \rightarrow \pi(p_3)K^*(p_4)$ are $a_{1/2} = 3\mathcal{M}_3^s - 2\mathcal{M}_3^t$ and $a_{3/2} = \mathcal{M}_3^t$. Here, $\mathcal{M}_3^s = \mathcal{M}_{(3-a)} + \mathcal{M}_{(3-b)}$, and

$\mathcal{M}_3^t = \mathcal{M}_{(3-c)} + \mathcal{M}_{(3-f)}$ are given as follows:

$$\begin{aligned} \mathcal{M}_3^s &= g_{K_1 K \rho} g_{K^* K \pi} \epsilon_1^\mu \epsilon_2^\nu \epsilon_4^{*\lambda} \frac{1}{s - m_K^2} (2p_3 + p_4)_\lambda \\ &\quad + g_{K_1 K_1 \rho} g_{K_1 K \pi} \epsilon_1^\mu \epsilon_2^\nu \epsilon_4^{*\lambda} \frac{-g_\lambda^{\mu'} + (p_1 + p_2)^{\mu'} (p_1 + p_2)_\lambda / m_{K_1}^2}{s - m_{K_1}^2} [g_{\mu'\nu} (p_1 + p_2)_\mu - g_{\mu\mu'} (p_1 + p_2)_\nu + g_{\mu\nu} p_{2\mu'}], \\ \mathcal{M}_3^t &= g_{K_1 K^* \pi} g_{\rho \pi \pi} \epsilon_1^\mu \epsilon_2^\nu \epsilon_4^{*\lambda} \frac{1}{t - m_\pi^2} (p_1 - 2p_3)_\mu \\ &\quad - g_{K_1 a_1 K^*} g_{a_1 \rho \pi} \epsilon_1^\mu \epsilon_2^\nu \epsilon_4^{*\lambda} \frac{-g_\mu^{\nu'} + (p_1 - p_3)_\mu (p_1 - p_3)^{\nu'} / m_{a_1}^2}{t - m_{a_1}^2} [g_{\lambda\nu} p_{2\nu'} - g_{\nu\nu'} p_{2\lambda} - g_{\lambda\nu'} (p_1 - p_3)_\nu]. \end{aligned} \quad (14)$$

The isospin channels of $\rho(p_1)K_1(p_2) \rightarrow K(p_3)\rho(p_4)$ are $a_{1/2} = -3\mathcal{M}_3^s - \mathcal{M}_4^t + 2\mathcal{M}_4^u$ and $a_{3/2} = 2\mathcal{M}_4^t - \mathcal{M}_4^u$. Here, $\mathcal{M}_4^s = \mathcal{M}_{(4-a)} + \mathcal{M}_{(4-b)}$, $\mathcal{M}_4^t = \mathcal{M}_{(4-c)} + \mathcal{M}_{(4-d)}$, and $\mathcal{M}_4^u = \mathcal{M}_{(4-e)}$ are given as follows:

$$\begin{aligned} \mathcal{M}_4^s &= g_{K_1 K \rho} g_{\rho K K} \epsilon_1^\mu \epsilon_2^\nu \epsilon_4^{*\lambda} \frac{1}{s - m_K^2} (2p_3 + p_4)_\lambda \\ &\quad + g_{K_1 K_1 \rho} g_{K_1 K \rho} \epsilon_1^\mu \epsilon_2^\nu \epsilon_4^{*\lambda} \frac{-g_\lambda^{\mu'} + (p_1 + p_2)^{\mu'} (p_1 + p_2)_\lambda / m_{K_1}^2}{s - m_{K_1}^2} [g_{\nu\mu'} (p_1 + p_2)_\mu - g_{\mu\mu'} (p_1 + p_2)_\nu + g_{\mu\nu} p_{2\mu'}], \\ \mathcal{M}_4^t &= g_{K_1 K \rho} g_{\rho K K} \epsilon_1^\mu \epsilon_2^\nu \epsilon_4^{*\lambda} \frac{1}{t - m_K^2} (p_1 - 2p_3)_\mu \\ &\quad + g_{K_1 K_1 \rho} g_{K_1 K \rho} \epsilon_1^\mu \epsilon_2^\nu \epsilon_4^{*\lambda} \frac{-g_\mu^{\nu'} + (p_1 - p_3)_\mu (p_1 - p_3)^{\nu'} / m_{K_1}^2}{t - m_{K_1}^2} [g_{\nu\nu'} (p_1 - p_3)_\lambda - g_{\nu'\lambda} (p_1 - p_3)_\nu + g_{\lambda\nu} p_{2\nu'}], \\ \mathcal{M}_4^u &= g_{K_1 K \rho} g_{\rho \rho \rho} \epsilon_1^\mu \epsilon_2^\nu \epsilon_4^{*\lambda} \frac{-g_\nu^{\mu'} + (p_1 - p_4)^{\mu'} (p_1 - p_4)_\nu / m_\rho^2}{u - m_\rho^2} [g_{\mu\mu'} (2p_1 - p_4)_\lambda - g_{\mu'\lambda} (p_1 - 2p_4)_\mu - g_{\mu\lambda} (p_1 + p_4)_{\mu'}]. \end{aligned} \quad (15)$$

We keep the convention where particles 1 and 2 stand for initial-state mesons, and particles 3 and 4 stand for final-state mesons shown on the left and right sides of the diagrams, respectively. The Mandelstam variables $s = (p_1 + p_2)^2$, $t = (p_1 - p_3)^2$, and $u = (p_1 - p_4)^2$ have also been used.

To take into account the finite size of the hadrons when calculating amplitudes, we introduce form factors shown below at each interaction vertex for the u, t -channel and the s -channel, respectively,

$$F_{u,t}(\vec{q}) = \frac{\Lambda^2 - m_{ex}^2}{\Lambda^2 + \vec{q}^2}, \quad F_s(\vec{q}) = \frac{\Lambda^2 + m_{ex}^2}{\Lambda^2 + \omega^2}, \quad (16)$$

with m_{ex} being the mass of the exchanging particle at each diagram. In Eq. (16) \vec{q}^2 is the squared three-momentum transfer at t, u -channels, and ω^2 is the total energy of the incoming particles at the s -channel in the center of mass frame. On the other hand, we apply the following form factor for the four point contact interaction,

$$F_c(\vec{k}) = \left(\frac{\Lambda^2}{\Lambda^2 + \vec{k}^2} \right)^2, \quad (17)$$

where \vec{k} is the average of the squared three-momenta from the form factors for the given channels at each process. We set the cut off parameter $\Lambda = 1.8$ GeV [14].

The cross section after spin averaging is given by

$$\sigma = \frac{1}{64\pi s} \int dt \frac{\overline{\mathcal{M}}^2}{|p_{1cm}|^2} F^4, \quad (18)$$

with $\overline{\mathcal{M}}^2$ being the squared amplitude of all processes evaluated by averaging and summing over the degeneracies of the initial and final particles, respectively. p_{1cm} in Eq. (18) represents for the three momenta of the initial particles in the center of mass frame. Fig. 2 shows the cross section for the absorption of the K_1 meson by π and ρ mesons.

For the hadronic production cross section of the K_1 meson during the hadronic stage in heavy-ion collisions, we will use detailed balance relation in the rate equation.

IV. TIME EVOLUTION OF THE K_1 MESON ABUNDANCE

We now investigate the time evolution of the K_1 meson abundance using the cross sections evaluated in the previous section. We construct an evolution equation, similar to that in Ref. [15], composed of densities and abundances for mesons participating in all the processes shown in Fig. 2: the dissociation processes of K_1 are due to π and ρ mesons.

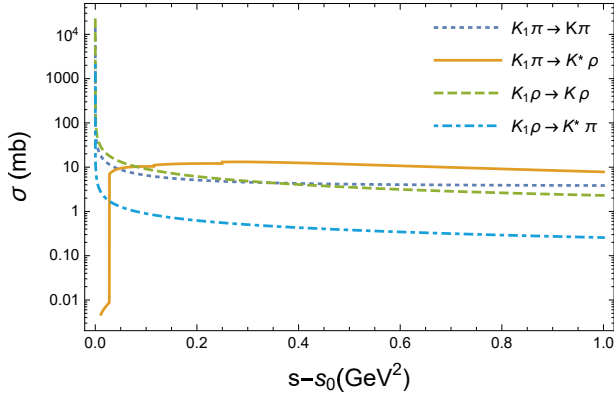


FIG. 2. The cross sections for the dissociation of the K_1 meson by π and ρ mesons via processes $K_1\pi \rightarrow K\pi$, $K_1\pi \rightarrow K^*\rho$, $K_1\rho \rightarrow K\rho$ and $K_1\rho \rightarrow K^*\pi$.

$$\begin{aligned}
\frac{dN_{K_1}(\tau)}{d\tau} = & \langle \sigma_{K_1\pi \rightarrow K\pi} v_{K_1\pi} \rangle n_\pi \left[-N_{K_1} + \frac{N_{K_1}^T}{N_K^T} N_K \right] \\
& + \langle \sigma_{K_1\pi \rightarrow K^*\rho} v_{K_1\pi} \rangle \left[-n_\pi N_{K_1} + \frac{n_\pi^T N_{K_1}^T}{n_\rho^T N_{K^*}^T} n_\rho N_{K^*} \right] \\
& + \langle \sigma_{K_1\rho \rightarrow K^*\pi} v_{K_1\rho} \rangle \left[-n_\rho N_{K_1} + \frac{n_\rho^T N_{K_1}^T}{n_\pi^T N_{K^*}^T} n_\pi N_{K^*} \right] \\
& + \langle \sigma_{K_1\rho \rightarrow K\rho} v_{K_1\rho} \rangle \left[-n_\rho N_{K_1} + \frac{n_\rho^T N_{K_1}^T}{n_\rho^T N_K^T} n_\rho N_K \right] \\
& + \langle \Gamma_{K_1 \rightarrow K\rho} \rangle \left[-N_{K_1} + \frac{N_{K_1}^T}{n_\rho^T N_K^T} n_\rho N_K \right] \\
& + \langle \Gamma_{K_1 \rightarrow K^*\pi} \rangle \left[-N_{K_1} + \frac{N_{K_1}^T}{n_\pi^T N_{K^*}^T} n_\pi N_{K^*} \right], \quad (19)
\end{aligned}$$

with $n_i(\tau)$ being the density of the light meson i in the hadronic phase at proper time τ . $N_j(\tau) = n_j(\tau)V(\tau)$, where $V(\tau)$ is the volume of the hadronic matter given in Eq. (27). The ones with the superscript T are the thermal abundance at temperature T , which depends on the proper time τ as given in Eq. (27).

$$\begin{aligned}
n_i^T(\tau) = & \frac{g_i}{2\pi^2} \int_0^\infty \frac{p^2 dp}{\exp(\sqrt{p^2 + m_i^2}/T(\tau)) - 1} \\
\approx & \frac{g_i}{2\pi^2} m_i^2 T(\tau) K_2 \left[\frac{m_i}{T(\tau)} \right], \quad (20)
\end{aligned}$$

where K_2 is the modified Bessel function of the second kind. We take $n_i(\tau) = n_i^T(\tau)$ for pions and ρ mesons.

We use the following two constraint equations involving the τ dependence for the numbers of K and K^* .

$$N_{K_1} + N_{N_{K^*}} + N_K = N_0, \quad (21)$$

$$\frac{N_{K^*} + N_{K_1} \times \text{BR}}{N_0} = aT + b, \quad (22)$$

where N_0 is a constant determined at the chemical freeze-out point. Eq. (21) follows from neglecting strangeness annihilation during the hadronic phase. $\text{BR}=0.16$ is the branching ratio of K_1 decaying into K^* so that the ratio in Eq. (22) is the ratio between the final K^* and K numbers when these mesons freeze-out at temperature T . This equation is motivated by the experimental observation that show the approximately linear decrease in the observed ratio between K^* and K numbers as a function of the cube root of multiplicity in heavy ion collision [16], which can be understood in a hadronic model calculation [15] that finds the ratio to decrease linearly with the temperature of the hadronic phase. The coefficients a and b in Eq. (22) were determined to reproduce the statistical model prediction for the ratio at $T = T_c$ and its linear reduction to 0.158 at $T = 90$ MeV, which are the observed values for the ratio and the extracted freeze-out temperature [24] for the lowest and highest centrality Pb-Pb collision [16], respectively. $a = 1.816$ GeV^{-1} and $b = -0.005444$ are obtained for the first scenario, where we assume that the number of K_1 is equal to that of K^* at the chemical freeze-out point, whereas $a = 2.272$ GeV^{-1} and $b = -0.04643$ in the second scenario, where we assume that both yields of K_1 and K^* follow statistical model values at the chemical freeze-out point. Solving Eq. (19) with the two constraints given in Eq. (21) and Eq. (22), we can determine the τ dependence and the final freeze-out numbers of N_{K_1} , N_{K^*} , N_K .

When substituting in the rate equation, we take the degeneracy factor $g_i = (2S + 1)$, where S is the spin, as the isospin effect is taken into account in the cross section which includes the contribution from all charge states. The production contribution has been taken into account by a detailed balance condition, which requires each square bracket in Eq. (19) to be zero in thermal equilibrium.

In Eq. (19), we have considered the thermally averaged cross section, $\langle \sigma_{ab \rightarrow cd} v_{ab} \rangle$ given below for initial two particles in a two-body process $ab \rightarrow cd$,

$$\begin{aligned}
\langle \sigma_{ab \rightarrow cd} v_{ab} \rangle = & \frac{\int d^3\vec{p}_a d^3\vec{p}_b f_a(\vec{p}_a) f_b(\vec{p}_b) \sigma_{ab \rightarrow cd} v_{ab}}{\int d^3\vec{p}_a d^3\vec{p}_b f_a(\vec{p}_a) f_b(\vec{p}_b)} \\
= & [64\pi T m_a^2 m_b^2 K_2(m_a/T) K_2(m_b/T)]^{-1} \\
& \times \int_{\sqrt{s_0}}^\infty d\sqrt{s} K_1(\sqrt{s}/T) \int_{t_0}^{t_1} dt |\mathcal{M}|^2, \quad (23)
\end{aligned}$$

with $\sqrt{s_0} = \max(m_a + m_b, m_c + m_d)$, K_1 and K_2 being the modified Bessel function of the second kind. The integration limits are $t_0(t_1) = (\frac{m_1^2 + m_3^2 - m_2^2 + m_4^2}{2\sqrt{s}})^2 - (p_{1cm} \mp p_{3cm})^2$. Here, we approximate f_i to be the Boltzmann momentum distribution of a particle i , $f_i(\vec{p}) = e^{-\sqrt{p^2 + m^2}/T}$. v_{ab} is the relative velocity of particles of species a and b , $v_{ab} = \sqrt{(p_a \cdot p_b)^2 - m_a^2 m_b^2} / (E_a E_b)$. $\langle \Gamma_{K_1} \rangle = \Gamma_{K_1}(m_{K_1}) K_1(m_{K_1}/T) / K_2(m_{K_1}/T)$ is the thermally averaged decay width of the K_1 meson [15].

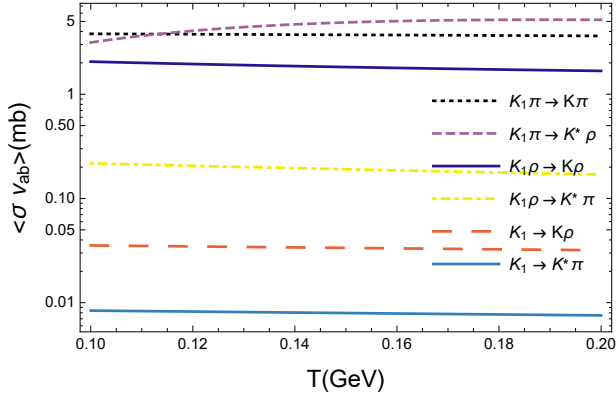


FIG. 3. Thermally averaged cross sections for the absorption of a K_1 meson via processes $K_1\pi \rightarrow K\pi$, $K_1\pi \rightarrow K^*\rho$, $K_1\rho \rightarrow K\rho$, $K_1\rho \rightarrow K^*\pi$, $K_1 \rightarrow K\rho$, and $K_1 \rightarrow K^*\pi$.

V. INITIAL TEMPERATURE AND TIME EVOLUTION IN HEAVY ION COLLISION

The initial temperature inside the nuclear matter produced from heavy ion collisions is studied with hydro simulation. We will consider Pb-Pb collision at $\sqrt{s_{NN}} = 5.02$ TeV in different centrality ranges: 0–5 %, 40–50 % and 70–80 %. The initial energy density in the transverse plane is calculated by using a two-dimensional Gaussian distribution of $\sigma = 0.4$ fm for each participating nucleon obtained from the Monte Carlo Glauber framework [17]. A scale factor as a function of the number of participating nucleons is multiplied to the initial density for a hydrodynamic evolution with the SONIC model [18]. This tune is required to match the multiplicity with the measured data in various centrality ranges [19].

Figure 4 shows the initial temperature distribution at $\tau_0 = 0.5$ fm/c of example events in three centrality ranges from the hydrodynamic simulation. As can be seen in the figure, the fraction of area where initial temperature is higher than 156 MeV is 84 %, 75 %, and 67 % in the 0–5 %, 40–50 %, and 70–80 % centrality ranges, respectively. Furthermore, the fraction of initial energy that comes from regions where the temperature is higher than 156 MeV is larger than 98% in all three centrality ranges. Therefore we can assume that almost all K_1 and K^* are produced through the QGP phase even in 70–80 % central collisions.

For calculation of the number of K_1 and K^* mesons inside the expanding medium, a more simple approach is used by assuming an isentropic expansion of uniform matter as follows [20]:

$$\partial_\tau(A\tau\langle T^{\tau\tau} \rangle) = -pA, \quad (24)$$

$$\partial_\tau(A\tau s\langle \gamma_r \rangle) = 0, \quad (25)$$

where $T^{\tau\tau} = (e+p)u_\tau^2 - p$ is the energy momentum tensor

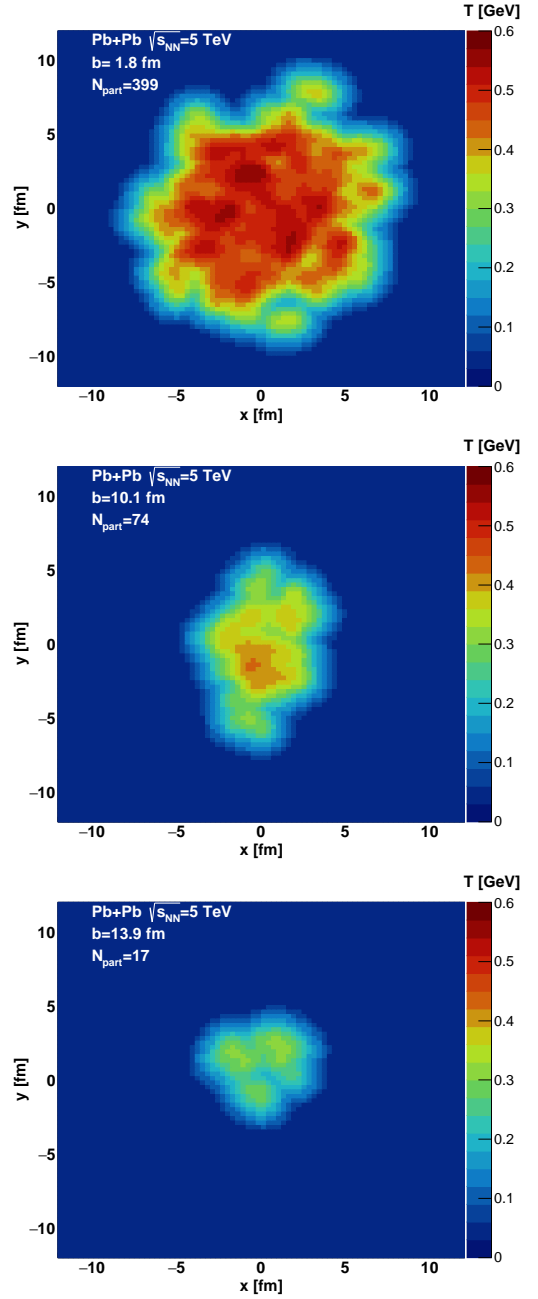


FIG. 4. Initial temperature distribution for example events in 0–5%, 40–50% and 70–80% centrality ranges of Pb-Pb collisions at $\sqrt{s_{NN}} = 5.02$ TeV.

in the Milne coordinate system with u_τ , e and p being the fluid velocity, energy density and pressure, respectively. s is the entropy density, $\gamma_r = 1/\sqrt{1-v_r^2}$ with v_r being the radial velocity of fluid cell, $A = \pi R^2$ with R being the transverse radius of the uniform matter and $\langle \dots \rangle$ denotes average over the transverse area. Eq. (25) clearly shows that the total entropy is conserved during the expansion with Lorentz contraction of transverse area due to the flow velocity taken into account.

It should be noted that while the entropy conservation is a reasonable approximation for the QGP phase, the effect of larger viscosity has to be taken into account for the hadronic phase[21]. While the simple hydrodynamic model could be supplemented through hadronic transport models to take into account the increase of entropy during the hadronic phase[22], we will leave such improvements for later study and neglect such effects in this work as the main tendency of the enhancement as a function of centrality will remain valid.

Assuming that the radial flow velocity is a linear function of the radial distance from the center, i.e., $\gamma_r v_r = \gamma_R \dot{R}(r/R)$, where $\dot{R} = \partial R / \partial \tau$ and $\gamma_R = 1 / \sqrt{1 - \dot{R}^2}$, we then have [20]

$$\begin{aligned} \langle u_\tau^2 \rangle|_{\eta=0} &= \langle \gamma_r^2 \rangle = 1 + \frac{\gamma_R^2 \dot{R}^2}{2}, \\ \langle \gamma_r \rangle &= \frac{2}{3\gamma_R^2 \dot{R}^2} (\gamma_R^3 - 1). \end{aligned} \quad (26)$$

Since the energy density e and pressure p are related by the equation of state of the matter through its temperature T [23], Eqs.(24)-(25) are thus simultaneous equations for T , \dot{R} .

The results of the numerical calculations can be parametrized in the following form for the hadronic phase:

$$\begin{aligned} V(\tau) &= \pi \left[R + v(\tau - \tau_c) + a/2(\tau - \tau_c)^2 \right]^2 \tau_c, \\ T(\tau) &= T_c - (T_h - T_f) \left(\frac{\tau - \tau_h}{\tau_f - \tau_h} \right)^\alpha, \end{aligned} \quad (27)$$

with T_h and T_f being the hadronization and kinetic freeze-out temperature. We take $T_h = 156$ MeV to be the same as the cross over temperature $T_c = T_h$. Eq. (27) can be thought to describe the system of the hadronic phase of the nuclear matter expanding with transverse velocity v and transverse acceleration a starting from its transverse size R at the chemical freeze-out time τ_c . The values of T_f according to centrality are taken from Ref. [24]. The values used in Eq. (27) are summarized in Table II. The schematic hydrodynamics in Eqs. (24) - (26) assumes the expansion of a uniform matter whose temperature or particle density is the same anywhere in the local rest frame. In the Lab. frame, however, the particle density increases with the radial distance due to Lorentz contraction. We note that Eq. (27) is not the parametrization for the volume in the Lab frame but for the volume with the Lorentz contraction taken into account, that is, $A\tau \langle \gamma_r \rangle$ in Eq. (25).

VI. THE ABUNDANCE OF K_1 MESONS IN HEAVY-ION COLLISIONS

Table III shows the abundance of the strange mesons at the chemical freeze-out point for different centrality ranges. The yield ratio between the K_1 and K^* mesons

TABLE II. Values for the volume and temperature profiles in the phenomenological model Eq.(27).

Centrality (%)	T_f (MeV)	t_c (fm/c)	t_f (fm/c)	R (fm)	v (c)	a (c^2/fm)	α
0 - 5%	90	8.7	28.1	14.9	0.93	0.04	0.835
40 - 50%	108	4.9	13	7.8	0.78	0.052	0.9
70 - 80%	147	2.2	2.9	4.43	0.481	0.161	0.847

at the kinetic freeze-out point is also given. N_{K_1} is the solution of the rate equation Eq. (19) with the initial number equal to $N_{K^*} = N_{K^*}^T$ at $T_c = 156$ MeV in the presence of chiral symmetry restoration. On the other hand, $N_{K_1}^T$ is the expected yield without chiral symmetry restoration when the initial number is given by its thermal equilibrium number at T_c . Hence, $N_{K_1}^T$ at the kinetic freeze-out point is the number expected in the statistical model when hadronic dissociation is taken into account. For a clear signature of chiral symmetry restoration at T_c , we want N_{K_1}/N_{K^*} at the kinetic freeze-out temperature to be sufficiently larger than $N_{K_1}^T/N_{K^*}$ at T_c , which is the standard statistical model prediction for the ratio. One notes that this is true for 40-50 % and 70-80 % centrality ranges. In fact, as can be seen in the last column of Table III, for 70-80 %, one finds that N_{K_1}/N_{K^*} at the kinetic freeze-out point is 0.905, which is much larger than $N_{K_1}^T/N_{K^*}$ at any time for all centralities: the time dependencies of $N_{K_1}^T$ and N_{K^*} are given in Fig. 5. Fig. 6 summarizes the yield ratios between K_1 and K^* mesons for different centralities with (red dots) and without (black squares) chiral symmetry restoration at T_c . As can be seen in the figure, the ratio increases sharply as the centrality decreases (because of the higher kinetic freeze-out temperature and thus the shorter lifetime of the hadronic phase at more peripheral collisions [25, 26]) when chiral symmetry restoration at T_c is taken into account. It is possible that at the chemical freeze-out point, the chiral order parameter will partly acquire its vacuum value. Then, the initial ratio of N_{K_1}/N_{K^*} at T_c would be slightly less than 1. Furthermore, the number of pions and rho mesons should be larger than estimated in Eq. (20) due to the effective chemical potential during the hadronic phase[27], leading to slightly larger dissociation cross sections than estimated in this work. Nevertheless, the large increase in the yield ratio towards peripheral collisions would still be visible so that one can identify chiral symmetry restoration. Hence, a systematic study of the ratio N_{K_1}/N_{K^*} for different centralities in a heavy ion collision will unambiguously show the evidence of chiral symmetry restoration at T_c .

VII. SUMMARY

We studied effects of chiral symmetry restoration at the chemical freeze-out point in a relativistic heavy ion

TABLE III. The kaon, K^* and K_1 meson abundances under hadronic interaction at chemical and kinetic freeze out temperatures. $N_{K_1}^T$ is the number of K_1 meson assuming thermal equilibrium while N_{K_1} is the abundance assuming chiral symmetry at T_c . The last column shows our prediction when chiral symmetry is restored.

Centrality	T(MeV)	N_K	N_{K^*}	$N_{K_1}^T$	N_{K_1}	$\frac{N_{K_1}^T}{N_{K^*}}$	$\frac{N_{K_1}}{N_{K^*}}$
0 – 5%	156	80.5	37.0	5.62	37.0	0.152	1.00
	90			0.157	1.37	0.006	0.057
40 – 50%	156	12.4	5.72	0.867	5.72	0.152	1.00
	108			0.149	1.17	0.034	0.268
70 – 80%	156	1.80	0.827	0.125	0.827	0.152	1.00
	147			0.108	0.714	0.137	0.905

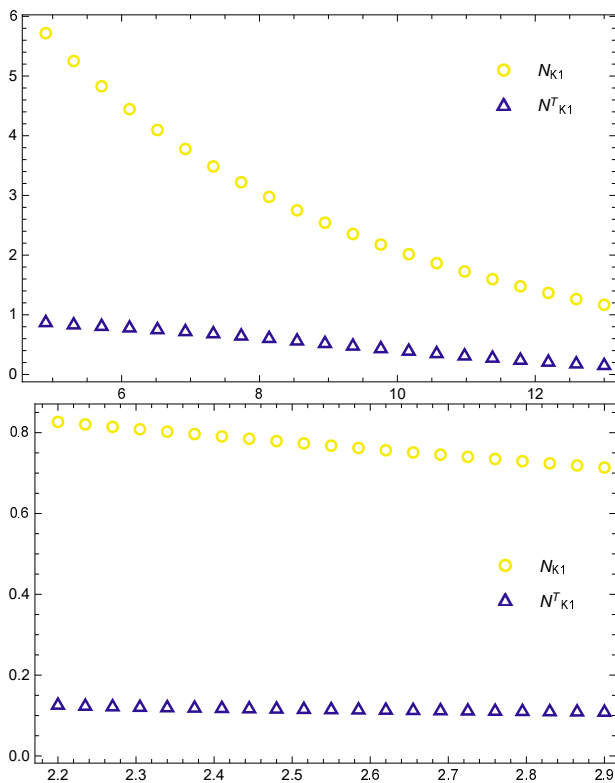


FIG. 5. The time evolution of the K_1 meson abundance under hadronic interaction when the initial number is equal to N_{K^*} (circle) or $N_{K_1}^T$ (triangle) at T_c for 40-50%(upper graph) and 70-80%(lower graph) centrality ranges.

collision. As the mass differences between the chiral partners are order parameters of the chiral symmetry restoration, the production of the chiral pairs will be degenerate at the chemical freeze-out point, where the chiral order parameter is found to be substantially reduced from the vacuum value in lattice calculations. For the effects to be observable, the vacuum width as well as the hadronic dissociation of both particles should be small so that the

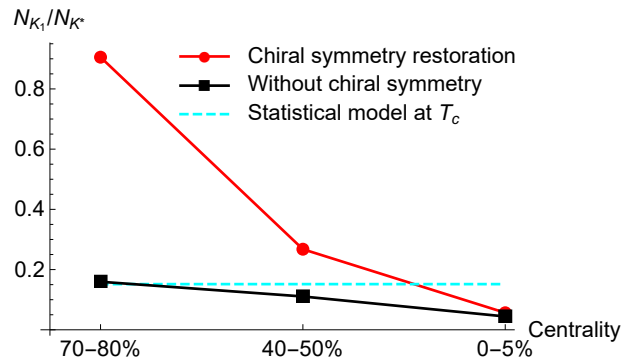


FIG. 6. The yield ratio of K_1 over K^* with and without chiral symmetry restoration for 70-80%, 40-50%, and 0-5% centrality ranges. K_1 feed down to K^* should be added when comparing to experiment.

signal will not be smeared out during the hadronic phase. The vacuum widths of both the K_1 and K^* meson are smaller than 100 MeV and thus potential candidates to be studied. We have performed a systematic study on their hadronic absorption during the hadronic phase as well as on the centrality dependence of these effects in a heavy ion collision. Our findings suggest that while the anomalously large initial ratio between the K_1 and K^* meson compared to that of the statistical model prediction will most likely be smeared out in a central collision, the signal will be visible in a peripheral heavy ion collision due to the shorter life time of the hadronic phase and higher freeze-out temperature.

The chiral partnership between the K^* and K_1 exists between the same charge states when the baryon chemical potential is non-zero [9]. In ultra-relativistic heavy ion collisions, the initial state will have almost zero baryon chemical potential. Hence, one can compare the production of any of the charge states through the decay products given below or their charge conjugation. For the K_1 meson they are

$$K_1^- \rightarrow \begin{cases} \rho^0 K^- \\ \rho^- \bar{K}^0 \\ \pi^0 K^{*-} \\ \pi^- \bar{K}^{*0} \end{cases}, \quad \bar{K}_1^0 \rightarrow \begin{cases} \rho^+ K^- \\ \rho^0 \bar{K}^0 \\ \pi^+ K^{*-} \\ \pi^0 \bar{K}^{*0} \end{cases},$$

and for K^*

$$K^{*-} \rightarrow \begin{cases} \pi^0 K^- \\ \pi^- \bar{K}^0 \end{cases}, \quad \bar{K}^{*0} \rightarrow \begin{cases} \pi^+ K^- \\ \pi^0 \bar{K}^0 \end{cases}.$$

A systematic study of the production of these states depending on the centrality will lead us to identify chiral symmetry restoration in heavy ion collision.

ACKNOWLEDGMENTS

This work was supported by Samsung Science and Technology Foundation under Project Number SSTF-BA1901-04. S. Lim acknowledge support from the National Research Foundation of Korea (NRF) grant

funded by the Korea government (MSIT) under Contract No. NRF-2008-00458. S. Cho was supported by the National Research Foundation of Korea (NRF) grant funded by the Korea government (MSIT) (No. 2019R1A2C1087107).

-
- [1] A. Bazavov *et al.* [HotQCD], Phys. Lett. B **795**, 15-21 (2019).
- [2] S. Borsanyi *et al.* [Wuppertal-Budapest], JHEP **09**, 073 (2010).
- [3] A. Andronic, P. Braun-Munzinger, K. Redlich and J. Stachel, Nucl. Phys. A **904-905**, 535c (2013).
- [4] J. Stachel, A. Andronic, P. Braun-Munzinger and K. Redlich, J. Phys. Conf. Ser. **509**, 012019 (2014).
- [5] H. T. Ding, A. Bazavov, F. Karsch, Y. Maezawa, S. Mukherjee and P. Petreczky, PoS **LATTICE2013**, 157 (2014).
- [6] S. Weinberg, Phys. Rev. Lett. **18**, 507 (1967).
- [7] J. Kim and S. H. Lee, Phys. Rev. D **103**, no.5, L051501 (2021).
- [8] A. Andronic, P. Braun-Munzinger, J. Stachel, Nucl. Phys. A **772**, 167 (2006).
- [9] T. Song, T. Hatsuda and S. H. Lee, Phys. Lett. B **792**, 160-169 (2019).
- [10] W. Cassing, A. Palmese, P. Moreau and E. L. Bratkovskaya, Phys. Rev. C **93**, 014902 (2016).
- [11] S. H. Lee, JPS Conf. Proc. **26**, 011012 (2019).
- [12] U. G. Meissner, Phys. Rept. **161**, 213 (1988).
- [13] M. Suzuki, Phys. Rev. D **47**, 1252 (1993).
- [14] G. E. Brown, C. M. Ko, Z. G. Wu and L. H. Xia, Phys. Rev. C **43**, 1881-1892 (1991).
- [15] S. Cho and S. H. Lee, Phys. Rev. C **97**, no.3, 034908 (2018).
- [16] S. Acharya *et al.* [ALICE], Phys. Lett. B **802**, 135225 (2020)
- [17] M. L. Miller, K. Reygers, S. J. Sanders, and P. Steinberg, Ann. Rev. Nucl. Part. Sci. **57**, 205 (2007).
- [18] M. Habich, J. L. Nagle, and P. Romatschke, Eur. Phys. J. C **75**, 15 (2015).
- [19] ALICE Collaboration, J. Adam, et al., Phys. Lett. B **772**, 567 (2017).
- [20] T. Song, K. C. Han and C. M. Ko, Phys. Rev. C **83**, 024904 (2011).
- [21] N. Demir and S. A. Bass, Phys. Rev. Lett. **102**, 172302 (2009).
- [22] J. Xu and C. M. Ko, Phys. Lett. B **772**, 290-293 (2017).
- [23] S. Borsanyi, G. Endrodi, Z. Fodor, A. Jakovac, S. D. Katz, S. Krieg, C. Ratti and K. K. Szabo, JHEP **11**, 077 (2010).
- [24] S. Acharya *et al.* [ALICE], Phys. Rev. C **101**, no.4, 044907 (2020).
- [25] S. Cho, T. Song and S. H. Lee, Phys. Rev. C **97**, no. 2, 024911 (2018).
- [26] A. Motornenko, V. Vovchenko, C. Greiner and H. Stoecker, Phys. Rev. C **102**, no. 2, 024909 (2020).
- [27] R. Rapp and E. V. Shuryak, Phys. Rev. Lett. **86**, 2980-2983 (2001).